**INTERNATIONAL JOURNAL OF ADVANCED RESEARCH**
*International Peer-Reviewed Research Journal*
**ISSN (Online): 3106-7980 | ISSN (Print): 3106-7972**
**Volume 3 • Issue 7 • November 2026**

# PHYSICS AND CHEMISTRY OF DEFECT-TOLERANT PEROVSKITE MATERIALS: CONTROLLING CARRIER DYNAMICS, ION MIGRATION, AND INTERFACIAL RECOMBINATION FOR STABLE OPTOELECTRONICS

**Eman Shah[*1], Muhammad Ali[2], Faiza Tariq[3], Muhammad Asim[4]**

[*1] *Department of Physics, Islamia College Peshawar, Pakistan*
[2] *Department of Physics, Quaid-i-Azam University, Islamabad, Pakistan*
[3] *Department of Physics, Quaid-i-Azam University, Islamabad, Pakistan*
[4] *Physics Teacher, Government Boys High School Damote, Juglote Sai, Gilgit, Pakistan*

[*1]shahzarsikandar@gmail.com, [2]muhammadaliqau013@gmail.com, [3]faizatariqqau021@gmail.com, [4]muhammadasimfaiz143@gmail.com

**DOI:** https://doi.org/10.5281/zenodo.24102589

**Keywords**
*Halide perovskites; defect tolerance; carrier dynamics; ion migration; interfacial passivation; self-assembled monolayers; operational stability.*

**Article History**
*Received: 05 August 2026*
*Accepted: 19 October 2026*
*Published: 04 November 2026*

**Copyright** @Author
**Corresponding Author: ***
**Eman Shah**

**Abstract**

*Halide perovskite semiconductors have become important materials for optoelectronics. These materials can convert power with efficiency over 26 percent. This is impressive because they are made at temperatures. Low temperature processing creates a lot of defects. The number of defects ranges from $10^{11}$ to $10^{16}$ per centimeter. This situation is called a paradox. It is known as "defect tolerance." It happens because of the way the electrons are arranged in these materials. The band-edge orbital symmetry is inverted. The valence band maxima are antibonding. The dielectric screening is strong. All of these factors make the natural point defects not harmful. This review looks closely at the physics and chemistry behind defect tolerance in $AMX_3$ perovskites. It studies how point defects form and the energy needed for that. It also looks at how the lattice moves and how polarons form. These help to hide charged defects. The review examines how carriers recombine. This happens through bimolecular and Auger processes. The review classifies the natural point defects. It separates the ones that are harmless from the deep ones that cause problems. These deep ones are called -radiative killer centers. The review looks at how ions move. This movement happens because of energy needed. The energy ranges from 0.2 to 0.8 electron volts. The review also studies how the materials break down. This includes electric field screening, phase decomposition at interfaces and halide segregation from light. To fix these problems the review looks at solutions. These include making the materials thinner and using dual-phase engineering. A special focus is on self-assembled monolayers. These layers help protect the interface in perovskite solar cells. Carbazole-based monolayers, like 2PACz derivatives and co-assembly methods work well. They reduce the -radiative recombination at the interface. The best devices keep than 93 percent of their original efficiency*

*after 1,000 hours. This review connects defect physics with real-world interface engineering. It gives a plan for making perovskite optoelectronics for use, in the market.*

## 1. INTRODUCTION

Halide perovskite semiconductors with the formula AMX_3 where A is a monovalent organic or inorganic cation (CH3NH3+ [MA] HC(NH2)2+ [FA], Cs+) M is a divalent metal cation (Pb2+ Sn2+). X is a halogen anion (I-, Br-Cl-) have changed the way we think about modern optoelectronics (Han et al. 2019). Power conversion efficiencies (PCEs) in single-junction perovskite cells (PSCs) have gone up from 3.8% to more than 26% matching the performance of single-crystal silicon photovoltaics. In addition to cells halide perovskites also work very well in light-emitting diodes (LEDs) photodetectors and direct X-ray detectors (Chen & Zhou 2020).

The quick progress of metal halide perovskites has created a question in solid-state physics: even though they are made at low temperatures using solution methods that usually cause a lot of crystallographic defects (10^11 to 10^16 cm^-3) these materials have long charge-carrier diffusion lengths (>3 micrometers) high open-circuit voltages (V_OC) and carrier lifetimes that last for microseconds (Ye et al. 2021). In covalently bonded semiconductors (like GaAs, Si, CdTe) similar levels of defects create mid-gap trap states that cause serious non-radiative recombination and damage the device. Halide perovskites have an ability to deal with these issues called "defect tolerance," where the main native point defects do not create deep recombination centers inside the forbidden bandgap (Zhang et al. 2026).

To make these materials practical for the market we need to close the gap between their natural defect tolerance and long-term stability. Defect tolerance helps the flow of charge carriers despite having some point defects. The performance of the device is still limited by ion movement when under electric fields defects forming when exposed to light and heat and non-radiative recombination happening at grain boundaries and, between different layers (Hu et al. 2021). This review looks closely at the structure that causes defect tolerance how carriers recombine, how ions move and the best ways to protect the surfaces of these materials like using self-assembled monolayers (SAMs) to make sure the devices work well over time (Huang et al., 2021).

## 2. Electronic Structure and Microscopic Mechanisms of Defect Tolerance

### 2.1 Orbital Configuration and Inverted Band-Edge Symmetry

The electronic origins for defect tolerance in lead halide perovskites reside in the unique orbital configurations of their band edges. In classic tetrahedrally bonded semiconductors, like silicon or gallium arsenide, the valence band edge (VBM) contains bonding atomic orbitals and the conduction band edge (CBM) is constructed from antibonding atomic orbitals (Lee et al., 2026). When a coordination bond is disrupted by an atomic vacancy or structural dislocation in these conventional lattice systems, leaving behind dangling bonds that are no longer involved in any electronic interactions, unpassivated dangling bonds form electronic states that are located energetically between antibonding and bonding bands to land abruptly in the mid-gap region as recombination-active deep traps (Kim et al., 2026). In metal halide perovskites, the reverse holds true owing to the interplay of the metal s and p states with the halogen p states. Antibonding hybridization between lead 6s lone pair orbitals and iodine 5p orbitals limits the valence band maximum (VBM) (Kurchin et al., 2018). The conduction band minimum (CBM) is the antibonding hybridization of lead 6p and iodine 5p orbitals, modulated by the strong relativistic spin-orbit coupling (SOC) which reduces the CBM energy. With the VBM itself being antibonding, atomic vacancies (such as Schottky defect pairs V_A^- and V_X^+) tend to raise the energy of the non-bonding states into the valence or conduction band continua as resonant states,

or spread them out as shallow states positioned next to the band edges (Liang et al., 2021).

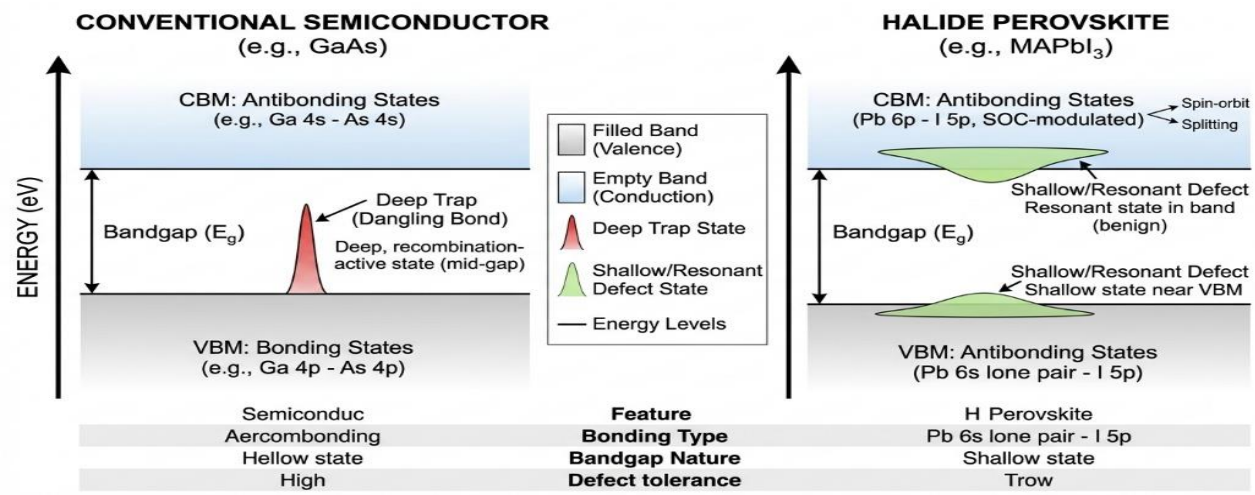



**Figure 1: Schematic comparison of orbital hybridization, band-edge symmetry, and defect trap behavior in conventional semiconductors versus metal halide perovskites.**

International Journal of Advanced Research

### 2.2 Thermodynamic Energetics of Point Defects

The equilibrium concentration $N_D$ of a defect $D$ in charge state $q$ is governed by its thermodynamic defect formation energy $\Delta H_f(D, q)$:

$$N_D = N_{sites} \exp\left(-\frac{\Delta H_f(D, q)}{k_B T}\right)$$

The formation energy is a dynamic quantity dependent on the chemical potentials $\mu_i$ of the constituent elements and the electronic Fermi level $E_F$:

$$\Delta H_f(D, q) = E(D, q) - E_{host} + \sum_i n_i \mu_i + q(E_F + E_V + \Delta V)$$

where $E(D, q)$ is the total energy of the supercell containing defect $D$ in charge state $q$, $E_{host}$ is the energy of the defect-free host crystal, $n_i$ is the number of atoms of type $i$ added ($n_i < 0$) or removed ($n_i > 0$), $E_V$ is the valence band maximum energy, and $\Delta V$ is the electrostatic alignment potential (Freysoldt et al., 2014).

The transition level $\varepsilon(q/q')$ between two charge states $q$ and $q'$ corresponds to the Fermi level position where the formation energies of both charge states are equal:

$$\varepsilon(q/q') = \frac{E(D, q) - E(D, q')}{q' - q}$$

In lead halide perovskites, low-energy native defects such as halogen vacancies V_X and cation vacancies V_A have formation energies that are conducive to their formation, yet their charge transition levels $\varepsilon(q/q')$ are found within the bands or just near to the band edges (Balasubramanian et al., 2018). In contrast, defects that give rise to deep transition levels close to mid-gap (for example, lead-in-iodine antisites "Pb"_"I" or interstitial iodine "I" _i) have significantly higher formation energies under along chemical potential range of stoichiometric synthesis conditions resulting in low equilibrium densities (Mosquera-Lois et al., 2023).

### 2.3 Dielectric Screening, Lattice Polarization, and Dynamic Disorder

Defect tolerance is reinforced by the dielectric response of the soft ionic perovskite structure. Perovskite halides have high- static (ε_s≈60 for 〖"MAPbI" 〗_3) or dynamic dielectric constants (Kumar et al., 2020), primarily through low-frequency optical phonons and large lattice polarization. The ions have inverse Born effective

charges (Z^*) that are larger than their expected oxidation states due to the redistribution of charges during the evolution of the metal halogen bonds (Anusca et al., 2017).

This coupling between defect states in halide perovskites (as ionized donors or acceptors) and the surrounding lattice can be explained by their high dielectric constants. This strong dielectric response reduces the Coulomb potential of charged defects and spreads out defect wavefunctions, and it ↓the electron-hole capture cross-sections (σ). Lattice polarization caused by high-energy symmetry lattice will form large polarons from photo-generated charge carriers, which move along the lattice with fantastic mobility trivially applicable to lost energy during defect trapping (Buixaderas et al., 2004).

Thermal fluctuations at room temperature give rise to dynamic structural disorder, leading to the corner-sharing MX_6^(4-) octahedra to tilt and distort in sub-picosecond timescales. This thermal motion generates temporal energetic fluctuations of defect levels by up to ∼1 eV A trap state that is momentary pushed into the mid gap region reverts back into the band continuum too fast for a carrier capture to take place and thus eliminates non-radiative recombination loops (Mattoni & Caddeo, 2020).

Table 1 provides a comparative summary of the electronic and structural properties that differentiate defect-tolerant halide perovskites from conventional semiconductors.

**Table 1: Electronic Band Edge Structure and Defect Dynamics Comparison**

| Parameter / Property | Conventional Semiconductors (e.g., GaAs, Si) | Metal halide perovskites (e.g., $MAPbI_3$, $FAPbI_3$) |
|---|---|---|
| **VBM Orbital Composition** | Bonding states (e.g., Ga 4p - As 4p) | Antibonding states (Pb 6s - I 5p) |
| **CBM Orbital Composition** | Antibonding states (e.g., Ga 4s - As 4s) | Antibonding states (Pb 6p - I 5p) with spin-orbit coupling |
| **Dangling Bond States** | Positioned near mid-gap (Deep killer traps) | Positioned inside bands or near band edges (Shallow/Resonant) |
| **Static Dielectric Constant ($\varepsilon_s$)** | Low to moderate (≈ 10–12) | High (≈ 30–60), dominated by lattice polarization |
| **Lattice Stiffness / Modulus** | Rigid, covalently bonded (> 100 GPa) | Soft, dynamically disordered ionic lattice (10–20 GPa) |
| **Dynamic Trap Fluctuations** | Static trap energy levels | Sub-picosecond energetic fluctuations (≤ 1 eV) |

## 3. Carrier Dynamics and Recombination Kinetics

### 3.1 Rate Equations and Recombination Coefficients

Charge carrier dynamics in halide perovskite absorbers following photo-excitation are governed by a polynomial differential equation that accounts for monomolecular, bimolecular, and trimolecular (Auger) recombination pathways:

$$\frac{dn}{dt} = G - k_1 n - k_2 n^2 - k_3 n^3$$

where n is the photogenerated carrier density G is the optical generation rate k_1 is the order monomolecular recombination rate constant k_2 is the second-order bimolecular recombination rate constant and k_3 is the third-order Auger recombination rate constant (La-o-vorakiat et al., 2015).

The total photo-generated carrier population, n, undergoes decay through three competing channels that depend on carrier density. Under solar illumination (1-sun intensity, corresponding to a steady-state carrier density of approximately $10^{15}$ $cm^{-3}$), monomolecular recombination via $k_1$ ($10^6$–$10^8$ $s^{-1}$) constitutes the principal energy loss channel (Peters et al., 2019). This first-order decay

reflects trap-assisted non-radiative Shockley–Read–Hall (SRH) recombination occurring at bulk point defects, grain boundaries, and heterojunction interfaces (Trimpl et al., 2020).

The rate constant $k_2$ (approximately $10^{-10}$ $cm^3$ $s^{-1}$) describes direct radiative recombination between free electrons and holes. While Langevin gas-phase theory predicts recombination rates for standard ionic systems, halide perovskites display a reduced $k_2$ value due to spatial charge separation induced by polarons and dynamic micro-domains (Yang et al., 2015).

The Auger rate $k_3$ ($10^{-28}$–$10^{-29}$ $cm^6$ $s^{-1}$) represents non-radiative three-body collisions in which the energy released by electron–hole annihilation is transferred as kinetic energy to a third charge carrier. Auger processes become dominant at high carrier densities ($n > 10^{17}$ $cm^{-3}$), such as those encountered in concentrated photovoltaics, high-power LEDs, and pulsed laser operation (Oki et al., 2017).

### 3.2 Shockley-Read-Hall Mechanics and Asymmetric Capture Coefficients

Multi-phonon emission in SRH kinetics concerns non-radiative capture. A neutral defect, $X^0$, captures a carrier by moving through a multi-dimensional potential energy surface associated with a classical coordinate shift ΔQ across an activation energy barrier E_t^n. Anharmonicity, which can arise from frequency shifts in localized phonons between charge states caused by changes in the shape of the potential energy surface, can increase or decrease E_th, thereby changing the carrier capture cross section (Whalley et al., 2021).

The efficiency of a defect center in annihilating charge carriers depends on its capture coefficients for both electrons ($k_n = \sigma_n v_{th}$) and holes ($k_p = \sigma_p v_{th}$), where $v_{th}$ is the thermal velocity (Sah, 1967). Maximum non-radiative recombination rates occur when the electron capture rate matches the hole capture rate:

$$nk_n = pk_p$$

When capture coefficients are strongly asymmetric ($k_n \gg k_p$ or $k_p \gg k_n$), a defect acts predominantly as a majority-carrier trap rather than a recombination center. In operating photovoltaic devices with asymmetric electron and hole concentrations across the absorber thickness, asymmetric capture dynamics suppress non-radiative recombination, expanding the energetic range over which defects remain benign (Das et al., 2020).

### 3.3 Carrier Diffusion Length and Lifetime Scaling

The effective charge-carrier lifetime τ is linked to the recombination coefficients via:

$$\tau = (k_1 + k_2 n + k_3 n^2)^{-1}$$

The ambipolar carrier diffusion length $L_D$ determines the average distance a photogenerated carrier traverses prior to recombination:

$$L_D = \sqrt{D\tau} = \sqrt{\frac{\mu k_B T}{q}\tau}$$

where D represents the carrier diffusion coefficient, μ denotes the charge carrier mobility, k_B is the Boltzmann constant, and q is the elementary charge (Gao et al., 2020). Targeted surface and grain-boundary passivation reduces k_1 by many orders of magnitude, pushing carrier lifetimes from less than 10 ns to more than 1 μs and improving L_D from less than a micron up to several microns which allows for the complete collection of charges from thick absorbers ( > 800 nm) (David,2021).

Table 2 outlines recombination rate constants, lifetimes, and carrier diffusion lengths across representative perovskite compositions and surface conditions.

Table 2: Carrier Recombination Parameters and Transport Metrics in Halide Perovskites

| System / Material Composition | $k_1$ ($s^{-1}$) | $k_2$ ($cm^3$ $s^{-1}$) | $k_3$ ($cm^6$ $s^{-1}$) | Carrier Lifetime $\tau$\tau$\tau$ | Diffusion Length LDL_DLD |
|---|---|---|---|---|---|
| $CsPbBr_3$ Pure Single Phase | $4.09 \times 10^7$ | $3.70 \times 10^{-10}$ | $6.75 \times 10^{-28}$ | ≈ 24.4 ns | ≈ 0.45 µm |
| $MAPbI_{3-x}Cl_x$ Solution Thin Film | $1.20 \times 10^7$ | $1.10 \times 10^{-10}$ | $2.30 \times 10^{-29}$ | ≈ 83.3 ns | ≈ 1.20 µm |
| $MA_{0.3}FA_{0.7}Pb_{0.5}Sn_{0.5}I_3$ (Control) | $3.30 \times 10^8$ | $3.50 \times 10^{-10}$ | $3.20 \times 10^{-28}$ | 3.0 ns | 0.75 µm |
| $MA_{0.3}FA_{0.7}Pb_{0.5}Sn_{0.5}I_3$ (Passivated) | $0.23 \times 10^8$ | $3.00 \times 10^{-10}$ | $3.50 \times 10^{-28}$ | 43.2 ns | 2.99 µm |
| Perovskite Film Unpassivated (Control) | $2.18 \times 10^8$ | $2.63 \times 10^{-13}$ | $4.18 \times 10^{-32}$ | ≈ 4.58 ns | < 0.50 µm |
| Perovskite Film Passivated (Additive) | $8.59 \times 10^7$ | $3.26 \times 10^{-13}$ | $1.07 \times 10^{-31}$ | ≈ 11.6 ns | > 1.10 µm |

## 4. Defect Physics, Ion Migration, and Degradation Pathways

### 4.1 Native Point Defects and Their Recombination Activity

Despite general defect tolerance, specific intrinsic point defects present in $AMX_3$ lattices can form deep electronic states if local hybridization conditions create strongly split bonding and antibonding levels within the bandgap (Xu et al., 2025). Intrinsic defects in halide perovskites fall into two distinct operational categories based on their electronic impact:

1. **Benign / Shallow Defects**: Halide vacancies ($V_X$) possess low formation energies under halogen-poor growth conditions. Although $V_X$ states predominantly lie shallow near the CBM, unpassivated clusters of halogen vacancies act as local electron traps and facilitate mass ion transport (Rahman et al., 2024). Cation vacancies ($V_A$, $V_M$) form shallow acceptor states near the VBM and contribute positively to p-type background conductivity without inducing non-radiative losses. Complex defect pairs, such as Schottky complexes ($2V_{Cu}^{-} + In_{Cu}^{2+}$) or combined stoichiometric vacancy units, similarly remain electrically inactive (Janotti & Van de Walle, 2007).

2. **Deep Recombination Centers**: Interstitial halides ($I_i$) and metal antisites ($Pb_I$, $I_{Pb}$) introduce deep levels near mid-gap. For example, the $Pb_I$ antisite defect in $CsPbI_3$ possesses deep transition levels across its $+1$, $+2$, and $+3$ charge states (Rezaei et al., 2024). Iodine interstitials ($I_i$) can transition between negative, neutral, and positive charge states, distorting the surrounding metal-halide octahedral framework and serving as rapid non-radiative recombination centers (Li et al., 2022).

### 4.2 Mechanisms and Kinetics of Ion Migration

The ionic nature and soft mechanical lattice of halide perovskites lead to low activation energies (E_a ≈ 0.2–0.8 eV) for point defect migration for halide vacancies (V_X^+). Under conditions such, as thermal stress, photo-excitation and applied electric fields, halide ions and vacancies move through interstitial sites or hopping pathways along grain boundaries (Pan et al. 2018).

This migration sets off a chain of chemical and electro-physical degradation processes. When an external electric field is. Under optical illumination mobile halide vacancies (V_X^+) move and gather at the electron and hole transport contacts (Lee et al., 2019). This buildup of charge blocks the built-in electric field (V_bi) changing the band bending near the contacts and causing strong current-voltage (J-V) hysteresis. Over time

the local loss of halides disrupts the crystal stoichiometry leading to phase decomposition into iodide ($PbI_2$) and volatile halogen gases. This breakdown speeds up performance degradation (Cao & Wang 2024).

Ion migration degrades device operation via several distinct pathways:

- **Internal Electric Field Screening**: Migrating ions accumulate at heterojunction interfaces, screening $V_{bi}$, altering band alignments, and inducing J-V hysteresis.
- **Interfacial Phase Decomposition**: Accumulated halogen ions react with metallic counter-electrodes (e.g., Ag, Cu), causing electrode corrosion and chemical degradation of the absorber layer (He et al., 2017).
- **Light-Induced Halide Segregation**: In mixed-halide perovskites (e.g., I/Br alloys used in tandem solar cells), photo-excitation drives phase separation into low-bandgap iodine-rich domains and high-bandgap bromine-rich domains, creating localized carrier traps that lower $V_{OC}$ (Lai et al., 2022).

**4.3 Suppression Strategies: Dimensionality and Dual-Phase Engineering**

Structural modification to raise the activation energy barrier for ion migration has been developed as a strategy to improve ion-migration barrier performance:

The shift from 3D to quasi two-dimensional (2D) structures - Ruddelsden-Popper or Dion-Jacobs - through the reduction of the crystal dimension with hydrophobic, sterically bulky organic spacer cations (for example phenylethylammonium[PEA] and butylammonium [BA]) raises the activation energy barrier. The presence of high formation energy of ionic vacancies inside the 2D quantum wells limits long-range ion diffusion within the 2D quantum wells (Su et al., 2026).

When a second crystallographic phase is present as a dual-phase 〖"CsPb" 〗_2 〖"Br" 〗_5/〖 "CsPbBr" 〗_3 composite, it acts to alleviate the local lattice strain, age the grain boundaries, and increase the barrier to halide ion migration. The exotic second phase effectively prevents dark leakage currents, and counteracts field-induced structural degradation of the perovskite lattice (Zhang et al., 2023).

**Table 3: Detailed Classification of Native Point Defects in Lead Halide Perovskites**

| Defect Notation | Defect Classification | Formation Energy (ΔHf\Delta H_fΔHf) Range | Trap Depth / Energy Level Position | Recombination Activity & Impact |
|---|---|---|---|---|
| $V_X$ (Halide Vacancy) | Native Vacancy | Low (Halogen-poor conditions) | Shallow donor (near CBM) | Benign electronically; primary driver of ion migration |
| $V_{Pb}$ (Lead Vacancy) | Native Vacancy | Low to Moderate (Pb-poor) | Shallow acceptor (near VBM) | Electrically benign; provides background p-type doping |
| $V_A$ (A-Site Vacancy) | Native Vacancy | Very Low | Shallow acceptor (within VB) | Benign; does not induce non-radiative loss |
| $I_i$ (Iodine Interstitial) | Native Interstitial | Moderate | Deep transition levels | Active non-radiative recombination center |
| $Pb_i$ (Lead Interstitial) | Native Interstitial | High | Deep donor trap | Recombination active; detrimental to lifetime |

| | | | | |
|---|---|---|---|---|
| $Pb_I$ (**Pb-on-I Antisite**) | Antisite Defect | High (Energetically unfavorable) | Deep trap (+1, +2, +3 states) | Severe killer center; distorts local octahedra |

**5. Interfacial Passivation and Self-Assembled Monolayers (SAMs) for Operational Stability**

**5.1 The Critical Role of Buried Interfaces**

Although the bulk absorbers have some intrinsic defect tolerance, the perovskite film-CTL (charge-blocking layer) interfaces usually contain higher defect densities: due to lattice mismatch, dangling bonds, a large number of noncoordinated ⟦"Pb" ^ (2+)" ions and stresses resulting from solvent evaporation. Interfacial non-radiative recombination is the main loss smaller than the Shockley-Queisser Radiative Limit in the open-circuit voltage (V_OC) (Yu et al., 2025).

To enable the identification of the buried interface defects to be overcome in inverted (p-i-n) PSCs, carbazole phosphonic acid derivative self-assembled monolayers (SAMs) have become effective hole-selective transport layers (HTLs). SAMs are directly deposited, polymer-free, into an ordered monomolecular arrangement on transparent conductive oxide (ITO or FTO) in place of conventional solution processed PEDOT: PSS or PTAA polymers (Zhang et al., 2026). Phosphonic acid anchors the SAM through the aliphatic chain to a conjugated carbazole core, and its crude structure is ended with specific functional groups that interact with the perovskite absorber during templated crystal growth (Hajimiri et al., 2026).

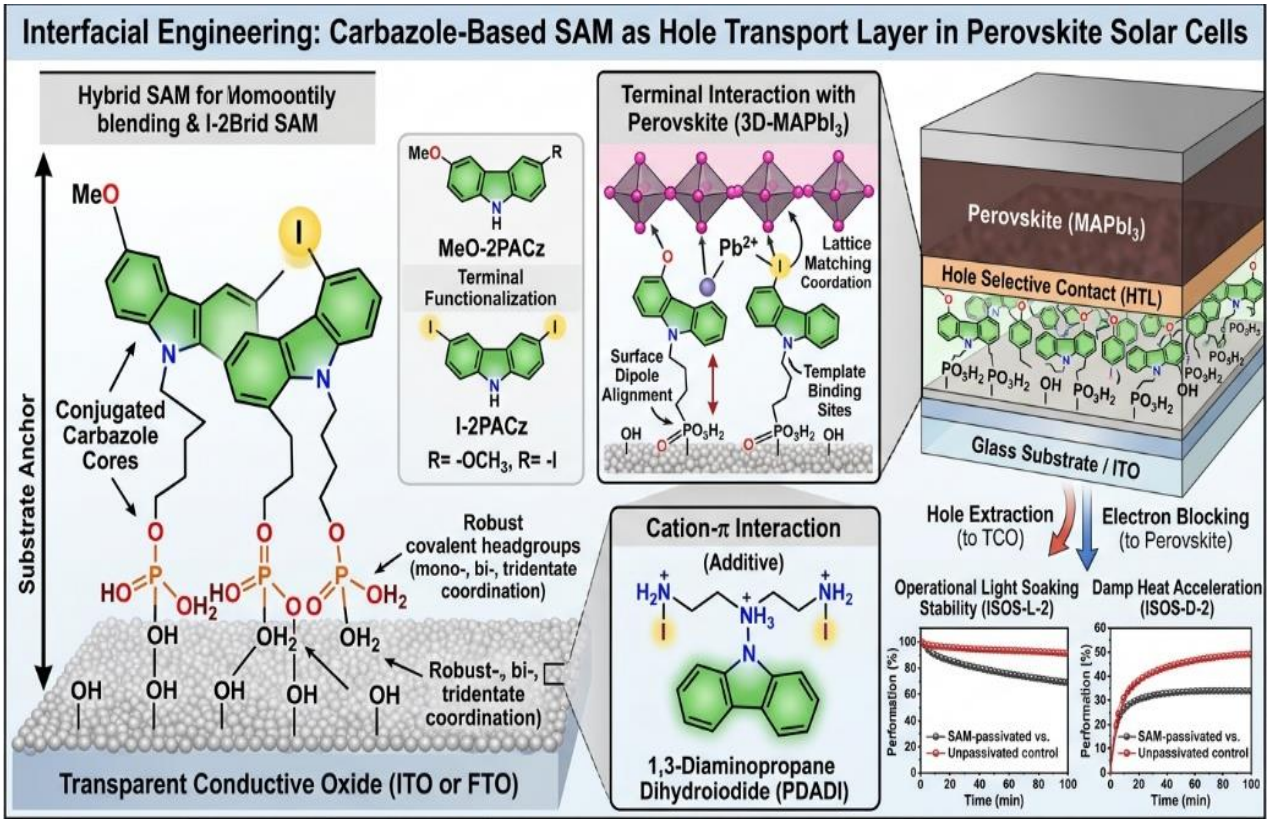



**Figure 2: Molecular architecture and co-assembly mechanism of carbazole-based self-assembled monolayers (SAMs) featuring phosphonic acid anchoring groups, conjugated cores, and terminal functionalization for buried interface passivation.**

### 5.2 Molecular Design Mechanics of Carbazole-Based SAMs

Carbazole-based SAM molecules such as [2-(9H-carbazol-9-yl) ethyl] phosphonic acid (2PACz), [2-(3,6-dimethoxy-9H-carbazol-9-yl) ethyl] phosphonic acid (MeO-2PACz), (2-(3,6-difluoro-9H-carbazol-9-yl) ethyl) phosphonic acid (F-2PACz), and halogenated variants (I-2PACz, Br-2PACz) consist of three functional units:

1. **Anchoring Group**: The phosphonic acid headgroup ($-PO_3H_2$) binds covalently to hydroxylated TCO surfaces via mono-, bi-, or tri-dentate coordination bonds. This reduces TCO surface states, enhances interfacial adhesion, and lowers contact resistance (Guo et al., 2024).

2. **Conjugated Carbazole Core**: The carbazole ring provides favorable π-electron delocalization, high intrinsic hole mobility, and strong chemical stability. Tuning carbazole substituents shifts the Highest Occupied Molecular Orbital (HOMO) energetic level, aligning it with the perovskite VBM to minimize energy offsets ($\Delta E_V$) and mitigate interfacial voltage loss (Tian et al., 2026).

3. **Terminal Functionalization**: Tailoring terminal groups (e.g., methoxy $-OCH_3$, halogen atoms $-I, -Br, -F$) modulates surface energy, wettability, and electronic work function. Methoxy groups ($-OCH_3$) increase surface dipole moments and improve precursor solution wetting, whereas halogenated terminals ($-I, -Br$) enhance interfacial lattice matching with perovskite crystals (Zhou et al., 20276).

### 5.3 Molecular Co-Assembly and Hybrid SAM Strategies

Pure single-component SAMs can suffer from molecular aggregation, non-uniform coverage on rough TCO surfaces, or asymmetric dipole interactions (Zhou et al., 2025). To overcome these challenges, co-assembly strategies blend two distinct functional molecules:

- **Carbazole SAM Blends**: Co-assembling MeO-2PACz and I-2PACz in tailored molar ratios breaks lateral symmetry, suppresses domain aggregation, and optimizes both hole extraction and surface coverage. The iodine moieties in I-2PACz provide periodic binding sites for perovskite nucleation, while MeO-2PACz establishes dipole alignment, eliminating energetic barriers (Wan et al., 2026).

- **Additive-Assisted Co-Assembly**: Integrating diammonium additives like 1,3-diaminopropane dihydroiodide (PDADI) with MeO-2PACz introduces cation-π interactions that disrupt intermolecular stacking. This increases SAM packing density, reduces pinhole formation, passivates uncoordinated $Pb^{2+}$ sites at the buried interface, and lowers residual tensile stress in the overlying perovskite absorber (Chi et al., 2026).

### 5.4 Accelerated Operational Stability Testing Under ISOS Standards

To evaluate commercial viability, SAM-passivated optoelectronic devices undergo testing adhering to International Summit on Organic Photovoltaic Stability (ISOS) standards:

- **ISOS-L-2 (Operational Light Soaking)**: Encapsulated devices featuring co-assembled SAMs (e.g., PDADI:MeO-2PACz) subjected to continuous 1-sun illumination under maximum power point tracking (MPPT) at 65 °C maintain over 93% of their initial PCE (champion PCE > 25.4%) after 1,000 hours of uninterrupted operation (Christians et al., 2018).

- **ISOS-D-2 (Damp Heat Acceleration)**: Unencapsulated devices modified with fluorinated or hydrophobic co-assembled SAMs subjected to 85 °C temperature and 85% relative humidity (RH) conditions retain over 91.4% of their initial capacity after 1,000 hours, whereas unpassivated control devices degrade below 50% capacity within 320 hours (Zhu et al., 2023).

Table 4 details key photovoltaic metrics and stability results achieved using various SAM hole transport configurations.

**Table 4: Key Performance and Operational Stability Parameters of Photovoltaic Devices Employing Various SAM Hole Transport Layers**

| Interfacial Strategy / SAM Composition | Device Geometry | Champion PCE (%) | Short-circuit current, J_SC (mA $cm^{-2}$) | Operational Lifetime & Protocol | Key Interfacial Mechanism |
|---|---|---|---|---|---|
| **MeO-2PACz (Pure Single Component)** | Inverted p-i-n | 24.21% | ≈ 24.50 | Retains 68% after 1000 h (ISOS-L-2) | High initial $V_{OC}$; limited by local molecular aggregation |
| **(MeO:I)-2PACz (Equimolar Co-Assembly)** | Inverted p-i-n | > 24.80% | ≈ 24.95 | Superior MPPT operational stability vs pure MeO | Balanced dipole alignment and reduced interfacial strain |
| **PDADI + MeO-2PACz (Hybrid SAM)** | Inverted p-i-n | 25.49% | 25.04 | Retains 93% after 1000 h (ISOS-L-2) | Cation-π interaction suppresses pinholes and passivates $Pb^{2+}$ |
| **PDADI + MeO-2PACz (Mini-Module 8.5 $cm^2$)** | Module p-i-n | 22.09% | Certified | High operational stability across large area | Uniform coating on large TCOs without pinhole defects |
| **Fluorinated SAM Passivation Layer** | Inverted p-i-n | > 26.00% | > 25.10 | Retains 91.4% after 1000 h (ISOS-D-2: 85°C/ 85% RH) | Hydrophobic barrier blocks moisture ingress and locks halide ions |

International Journal of Advanced Research

## 6. Conclusion

This review has examined the physics and chemistry that govern defect tolerance in halide perovskite materials building a full framework that links basic electronic structure to how devices perform and stay stable. The built-in defect tolerance of $AMX_3$ perovskites comes from their orbital set-up, where antibonding valence band traits and strong spin-orbit coupling push vacancy-induced states into band continua or shallow edges stopping deep mid-gap recombination centers that normally upset ordinary covalent semiconductors. A thermodynamic look at defect formation energies shows that low-energy native defects, such as halide and cation vacancies remain electrically harmless while deep-level antisites and interstitials have formation energies when the material is stoichiometric keeping those numbers low. The soft polarizable ionic lattice also boosts defect tolerance by giving screening forming large polarons and producing sub-picosecond dynamic trap changes that stop carriers from being captured. With these natural strengths getting to commercial use needs work on ion migration and interface recombination which are the main causes of operational decay. Halide vacancies move under fields and light gathering at heterojunction interfaces to block built-in potentials create J-V hysteresis and cause phase breakdown. Mixed-halide systems also suffer light-induced segregation that hurts steadiness. Self-assembled monolayers, carbazole phosphonic acid derivatives have become strong interface tools that both shield buried interface defects align energy levels and stop ion migration by using hydrophobic barriers and lattice-matching end groups. Co-assembly and hybrid SAM methods give even coverage and tight packing with PDADI:MeO-2PACz systems reaching 25.49 %

PCE and keeping 93 % after 1,000 hours under ISOS-L-2 tests. Future studies must focus on making multifunctional passivation molecules that heal defects, block ions and resist moisture; on spreading SAM approaches to panels and tandem designs; and on setting standard accelerated aging tests that truly predict real-world lifetimes. By joining defect physics, carrier motion and interface chemistry this review gives a design guide for new optoelectronics that use natural defect tolerance while building extra stability, for market use.

**REFERENCES**

Anusca, I., Balčiūnas, S., Gemeiner, P., Svirskas, Š., Sanlialp, M., Lackner, G., ... & Lupascu, D. C. (2017). Dielectric response: answer to many questions in the methylammonium lead halide solar cell absorbers. Advanced Energy Materials, 7(19), 1700600.

Balasubramanian, K., Khare, S. V., & Gall, D. (2018). Energetics of point defects in rocksalt structure transition metal nitrides: Thermodynamic reasons for deviations from stoichiometry. Acta Materialia, 159, 77-88.

Buixaderas, E., Kamba, S., & Petzelt, J. (2004). Lattice dynamics and central-mode phenomena in the dielectric response of ferroelectrics and related materials. Ferroelectrics, 308(1), 131-192.

Cao, D., & Wang, Y. (2024). Ion migration in metal halide perovskites: characterization protocols and physicochemical mechanisms. The Journal of Physical Chemistry Letters, 15(27), 6986-6995.

Chen, Y., & Zhou, H. (2020). Defects chemistry in high-efficiency and stable perovskite solar cells. Journal of Applied Physics, 128(6).

Chi, M., Cui, X., Xie, G., Fang, J., Ouyang, D., Wang, Y., ... & Liu, Y. (2026). Synergistic Hole-Selective Contact Enabling Highly Efficient Perovskite/Organic Tandem Solar Cells. Advanced Energy Materials, e70945.

Christians, J. A., Schulz, P., Tinkham, J. S., Schloemer, T. H., Harvey, S. P., Tremolet de Villers, B. J., ... & Luther, J. M. (2018). Tailored interfaces of unencapsulated perovskite solar cells for> 1,000 hour operational stability. Nature Energy, 3(1), 68-74.

Das, B., Aguilera, I., Rau, U., & Kirchartz, T. (2020). What is a deep defect? Combining Shockley-Read-Hall statistics with multiphonon recombination theory. Physical Review Materials, 4(2), 024602.

David, A. (2021). Long-range carrier diffusion in (In, Ga) N quantum wells and implications from fundamentals to devices. Physical Review Applied, 15(5), 054015.

Freysoldt, C., Grabowski, B., Hickel, T., Neugebauer, J., Kresse, G., Janotti, A., & Van de Walle, C. G. (2014). First-principles calculations for point defects in solids. Reviews of modern physics, 86(1), 253-305.

Gao, M., Liu, H., Yu, S., Louisia, S., Zhang, Y., Nenon, D. P., ... & Yang, P. (2020). Scaling laws of exciton recombination kinetics in low dimensional halide perovskite nanostructures. Journal of the American Chemical Society, 142(19), 8871-8879.

Guo, S., Yang, X., Zhang, Q., Jin, X., Zhang, D., Guo, Y., ... & Xu, B. (2024). Fused Carbazole-based Self-Assembled Monolayers Enable Efficient Perovskite Solar Cells and Perovskite Light-Emitting Diodes. Advanced Optical Materials, 12(33), 2401617.

Hajimiri, I., Shahroosvand, H., Bellani, S., Manna, L., & Nazeeruddin, M. K. (2026). Hole-selective self-assembled monolayers: a molecular platform for high-performance perovskite photovoltaics. Chemical Society Reviews.

Han, T. H., Tan, S., Xue, J., Meng, L., Lee, J. W., & Yang, Y. (2019). Interface and defect engineering for metal halide perovskite optoelectronic devices. Advanced Materials, 31(47), 1803515.

He, X., Zhu, Y., & Mo, Y. (2017). Origin of fast ion diffusion in super-ionic conductors. Nature communications, 8(1), 15893.

Hu, T., Li, D., Shan, Q., Dong, Y., Xiang, H., Choy, W. C., & Zeng, H. (2021). Defect behaviors in perovskite light-emitting diodes. ACS Materials Letters, 3(12), 1702-1728.

Huang, L., Ge, Z., Zhang, X., & Zhu, Y. (2021). Oxygen-induced defect-healing and photo-brightening of halide perovskite semiconductors: science and application. Journal of Materials Chemistry A, 9(8), 4379-4414.

Janotti, A., & Van de Walle, C. G. (2007). Native point defects in ZnO. Physical Review B Condensed Matter and Materials Physics, 76(16), 165202.

Kim, C., Kang, H., Jung, S., Molla, C. F., Jeong, J., Ambili, S., ... & Lee, J. (2026). Dimensionality and Chirality in Halide Double Perovskites: A Coupled Design Framework for Polarization Control. Advanced Optical Materials, e71929.

Kurchin, R. C., Gorai, P., Buonassisi, T., & Stevanovic, V. (2018). Structural and chemical features giving rise to defect tolerance of binary semiconductors. Chemistry of Materials, 30(16), 5583-5592.

Lai, Y., Xie, H., Li, P., Li, B., Zhao, A., Luo, L., ... & Cao, Y. (2022). Ion-migration mechanism: an overall understanding of anionic redox activity in metal oxide cathodes of Li/Na-ion batteries. Advanced Materials, 34(47), 2206039.

La-o-vorakiat, C., Salim, T., Kadro, J., Khuc, M. T., Haselsberger, R., Cheng, L., ... & Chia, E. E. (2015). Elucidating the role of disorder and free-carrier recombination kinetics in CH3NH3PbI3 perovskite films. Nature communications, 6(1), 7903.

Lee, J. W., Kim, S. G., Yang, J. M., Yang, Y., & Park, N. G. (2019). Verification and mitigation of ion migration in perovskite solar cells. APL materials, 7(4).

Lee, Y. M., Maeng, I., Park, J., Oh, S. J., & Jung, M. C. (2026). Band-like Carriers in a Soft, Anharmonic Lattice: Lead-Halide Perovskites. arXiv preprint arXiv:2608.28104.

Li, Y., Li, Z., Liu, F., & Wei, J. (2022). Defects and passivation in perovskite solar cells. Surface Innovations, 10(1), 3-20.

Liang, H., Xiang, H., Zhu, R., Liu, C., & Jia, Y. (2021). The structural stability and defect-tolerance of ionic spinel semiconductors for high-efficiency solar cells. Journal of Materials Chemistry A, 9(25), 14566-14575.

Mattoni, A., & Caddeo, C. (2020). Dielectric function of hybrid perovskites at finite temperature investigated by classical molecular dynamics. The Journal of Chemical Physics, 152(10).

Mosquera-Lois, I., Kavanagh, S. R., Klarbring, J., Tolborg, K., & Walsh, A. (2023). Imperfections are not 0 K: free energy of point defects in crystals. Chemical Society Reviews, 52(17), 5812-5826.

Oki, K., Ma, B., & Ishitani, Y. (2017). Population decay time and distribution of exciton states analyzed by rate equations based on theoretical phononic and electron-collisional rate coefficients. Physical Review B, 96(20), 205204.

Pan, D., Fu, Y., Chen, J., Czech, K. J., Wright, J. C., & Jin, S. (2018). Visualization and studies of ion-diffusion kinetics in cesium lead bromide perovskite nanowires. Nano letters, 18(3), 1807-1813.

Peters, J. A., Liu, Z., Yu, R., McCall, K. M., He, Y., Kanatzidis, M. G., & Wessels, B. W. (2019). Carrier recombination mechanism in CsPbB r 3 revealed by time-resolved photoluminescence spectroscopy. Physical Review B, 100(23), 235305.

Rahman, M. H., Biswas, M., & Mannodi-Kanakkithodi, A. (2024). Understanding defect-mediated ion migration in semiconductors using atomistic simulations and machine learning. ACS Materials Au, 4(6), 557.

Rezaei, M., Nezamzadeh-Ejhieh, A., & Massah, A. R. (2024). A comprehensive review on the boosted effects of anion vacancy in the heterogeneous photocatalytic degradation, part II: focus on oxygen vacancy. ACS omega, 9(6), 6093.

Sah, C. T. (1967). The equivalent circuit model in solid-state electronics Part I: The single energy level defect centers. Proceedings of the IEEE, 55(5), 654-671.

Su, M., Cao, Y., Zhang, M., Li, H., Zhang, C., Li, S., ... & Lu, Q. (2026). Synergistic Ostwald Ripening Suppression and Organic Acid Ligand Engineering for Micrometer-Scale β-FeOOH Nanorod Arrays as Ultrahigh-Capacity Lithium-Ion Battery Anodes. Small, 22(2), e10041.

Tian, J., Xie, Y., Tian, M., Chen, J., & Lv, M. (2026). Carbazole-Based Self-Assembled Monolayers for Hole Transport in Photovoltaics: A Molecular Engineering Perspective. Aggregate, 7(1), e70259.

Trimpl, M. J., Wright, A. D., Schutt, K., Buizza, L. R., Wang, Z., Johnston, M. B., ... & Herz, L. M. (2020). Charge-carrier trapping and radiative recombination in metal halide perovskite semiconductors. Advanced functional materials, 30(42), 2004312.

Wan, W., Gao, M., Ou, Z., Wang, C., Liu, L., Peng, D., ... & Jiang, T. (2026). Molecular interaction between hybrid self-assembled molecules enables high-performance inverted perovskite solar cells. Energy & Environmental Science, 19(17), 5797-5808.

Whalley, L. D., Van Gerwen, P., Frost, J. M., Kim, S., Hood, S. N., & Walsh, A. (2021). Giant Huang–Rhys factor for electron capture by the iodine intersitial in perovskite solar cells. Journal of the American Chemical Society, 143(24), 9123.

Xu, N., Qi, X., Shen, Z., Hu, L., Lv, J., Zhong, Y., ... & Zou, Z. (2025). Point defects in metal halide perovskites. Nature Reviews Physics, 7(10), 554-564.

Yang, Y., Yang, M., Li, Z., Crisp, R., Zhu, K., & Beard, M. C. (2015). Comparison of recombination dynamics in CH3NH3PbBr3 and CH3NH3PbI3 perovskite films: influence of exciton binding energy. The journal of physical chemistry letters, 6(23), 4688-4692.

Ye, J., Byranvand, M. M., Martínez, C. O., Hoye, R. L., Saliba, M., & Polavarapu, L. (2021). Defect passivation in lead-halide perovskite nanocrystals and thin films: toward efficient LEDs and solar cells. Angewandte Chemie International Edition, 60(40), 21636-21660.

Yu, X., Sun, X., Zhu, Z., & Li, Z. A. (2025). Stabilization Strategies of Buried Interface for Efficient SAM-Based Inverted Perovskite Solar Cells. Angewandte Chemie, 137(4), e202419608.

Zhang, C., Yin, Z., Shi, L., Chen, D., Yang, W., & Shang, M. H. (2026). Advancements and challenges of self-assembled monolayers as buried interfaces in inverted perovskite solar cells: from molecular design to automation-enabled data-driven optimization. Journal of Materials Chemistry A, 14(41), 27372-27393.

Zhang, L., Li, Z., Bi, Q. Q., Jiang, L. Y., Zhang, X. D., Tang, E., ... & Wang, D. Y. (2023). Strong yet tough epoxy with superior fire suppression enabled by bio-based phosphaphenanthrene towards in-situ formed Diels-Alder network. Composites Part B: Engineering, 251, 110490.

Zhang, Y., Fu, G., Liang, Z., Liu, S., & Park, N. G. (2026). Semiconductive Polarity Control in Halide Perovskites through Defect Chemistry and Interface Engineering. Advanced Energy Materials, e70691.

Zhou, H., Do, J. J., Jung, Y. H., Kang, H., Kwon, S., Kim, G. H., ... & Kang, S. H. (2025). Rational design strategy of co-self-assembled monolayers for high-efficiency and stable inverted perovskite solar cells. Chemical Engineering Journal, 511, 162010.

Zhou, S., Zhang, P., Han, L., Zhu, K., Cui, C., Bin, H., & Li, Y. (2026). Synergistic conformation locking and terminal conjugation engineering of carbazole-based self-assembled monolayers for high-performance organic solar cells. Science China Materials, 1-10.

Zhu, H., Teale, S., Lintangpradipto, M. N., Mahesh, S., Chen, B., McGehee, M. D., ... & Bakr, O. M. (2023). Long-term operating stability in perovskite photovoltaics. Nature Reviews Materials, 8(9), 569-586.

International Journal of Advanced Research